**Date of Experiment:** 11/11/2024
**Date of Report:** 17/12/2024

# Lab Report
# Magnetoresistance

**Experiment conducted by:** Syed Hussain Haider
**Lab Partner:** Arya Gonullu

**Abstract**

This experiment investigated the magnetoresistance (MR) characteristics of two types of Giant Magnetoresistance (GMR) sensors, a multilayer GMR sensor and a spin-valve GMR sensor. A Helmholtz coil arrangement was used to apply a uniform magnetic field, while a modified Wheatstone bridge circuit measured resistance changes as a function of the applied field. The spin-valve GMR sensor strongly agreed with theoretical expectations, exhibiting a well-defined linear range ($-0.8\,\mathrm{mT}$ to $0.8\,\mathrm{mT}$) and a sensitivity of $14.64\,\mathrm{mV/V/mT}$, consistent with predicted values. In contrast, the multilayer GMR sensor displayed deviations, including a delayed onset of the linear region and a reduced measured sensitivity ($16.72\,\mathrm{mV/V/mT}$) compared to the expected range of $30.0 - 42.0\,\mathrm{mV/V/mT}$. These discrepancies likely resulted from calibration issues or insufficient stabilization time during measurements. The experiment successfully demonstrated key MR phenomena and emphasized the importance of precise calibration and controlled measurement conditions to characterise GMR sensors accurately.

# 1 Introduction

Magnetoresistance (MR) is the phenomenon in which the electrical resistivity of a material is changed in response to an external magnetic field. It was first discovered by William Thomson (Lord Kelvin) in the 19th century. When a magnetic field is applied to a conductive material, conduction electrons are made to experience a Lorentz force that changes their trajectories. This deflection causes changes to the mean free path (the average distance an electron travels between collisions), leading to a change in the material's resistivity.

The conventional MR effect is known for small changes in resistivity. However, in the 1980s, the Giant Magnetoresistance (GMR) effect was discovered by Albert Fert and Peter Grünberg, for which they were awarded a Nobel Prize. The resistivity changes in the GMR effect are much larger than those in conventional MR. This is because GMR consists of thin-film layers made of alternating ferromagnetic and non-magnetic metallic layers, each only a few nanometers thick. These multilayer structures result in a much greater change in resistivity.

The aim of this experiment is to investigate magnetoresistance using two types of GMR sensors: the multilayer GMR and the spin-valve GMR. The multilayer GMR consists of multiple alternating layers of ferromagnetic and non-magnetic conductive materials (as shown in Figure 1). Typically, a multilayer GMR contains stacks of approximately 7 to 10 layers, each with a thickness of about 1 nm.

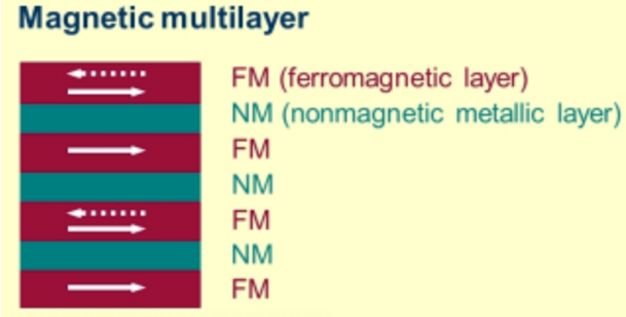


Figure 1: Schematic representation of the multilayer Giant Magnetoresistance (GMR) structure, illustrating alternating ferromagnetic (FM) and non-magnetic metallic (NM) layers. Adapted from Tsymbal and Pettifor [10].

In contrast, the spin-valve GMR is composed of a fixed (pinned) ferromagnetic layer and a free ferromagnetic layer, which are separated by a non-magnetic metallic layer. The pinned ferromagnetic layer is stabilized by placing an antiferromagnetic layer directly above it (as shown in Figure 2).

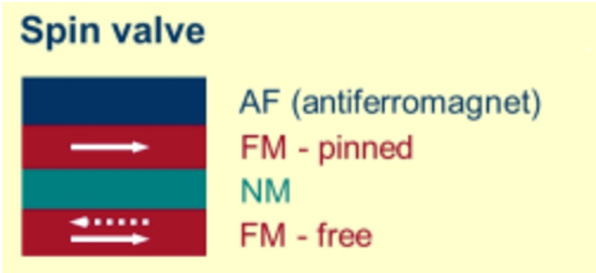


Figure 2: Schematic representation of the spin-valve Giant Magnetoresistance (GMR) structure, with a pinned ferromagnetic layer stabilized by an antiferromagnetic (AF) layer and a free ferromagnetic layer separated by a non-magnetic metallic layer. Adapted from Tsymbal and Pettifor [10].

## 2 Theory

Magnetoresistance is defined as the ratio of the change in resistivity of a material caused by applying a magnetic field to its resistivity when no magnetic field is present [4].

$$\frac{\Delta\rho}{\rho_0} = \frac{\rho_H - \rho_0}{\rho_0} \tag{1}$$

Where $\rho_H$ is the resistivity at magnetic field strength $H$, and $\rho_0$ is the resistivity in the absence of any magnetic field. Equation (1) can also be written as:

$$\frac{\Delta R}{R_0} = \frac{R_B - R_0}{R_0} \tag{2}$$

For a particular device, $R_B$ is the resistance at magnetic field strength $H$, and $R_0$ is the resistance without any magnetic field [4].

$R_B$ and $R_0$ were measured using a modified Wheatstone bridge. The configuration of the Wheatstone Bridge was adjusted as follows [8].

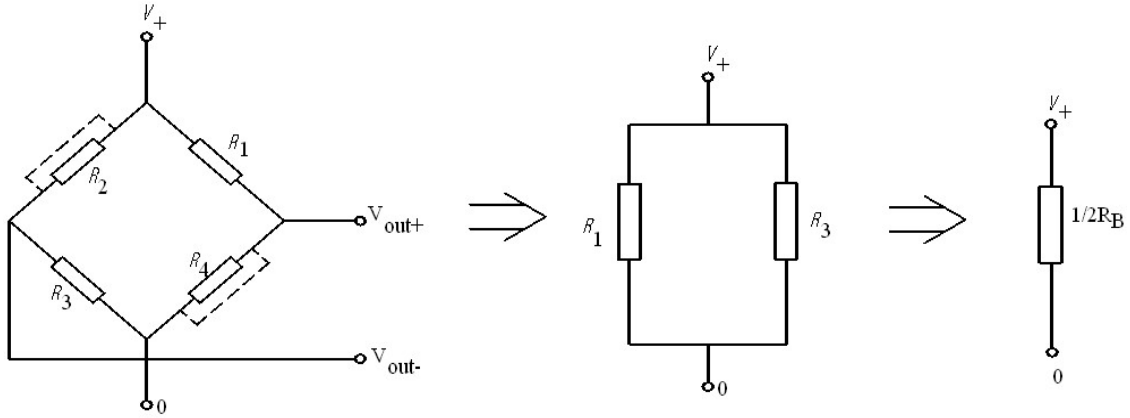


Figure 3: Modified Wheatstone Bridge configuration used to measure resistance changes in response to magnetic field strength. In this configuration, resistors $R_2$ and $R_4$, unaffected by the external magnetic field, are short-circuited by connecting $V_+$ to $V_{\text{out-}}$ and grounding $V_{\text{out+}}$. This simplifies the circuit to a parallel arrangement of $R_1$ and $R_3$, both of which vary with the magnetic field. The equivalent resistance is then reduced to $\frac{1}{2}R_B$ across $V_+$ and ground, where $R_B$ represents the resistance of the magnetoresistors under a given magnetic field. Adapted from Lambda Scientific [5].

The Wheatstone bridge consists of four resistors, $R_2$ and $R_4$, which is unaffected by the external magnetic field, and $R_1$ and $R_3$, whose resistances vary depending on the strength of the magnetic field. The rewiring simplifies the circuit by short-circuiting $R_2$ and $R_4$, ensuring they no longer influence the output measurement. $R_1$ and $R_3$ are then connected in parallel, reducing the total resistance to $\frac{1}{2}R_B$. This configuration allows precise measurement of the magnetoresistance response by isolating the resistors affected by the external magnetic field.

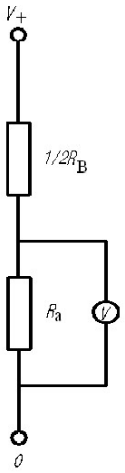


Figure 4: Simplified Wheatstone bridge circuit showing the equivalent resistance $\frac{1}{2}R_B$ across $V_+$ and ground. A resistor $R_a$ is connected in series with $\frac{1}{2}R_B$, and a voltmeter is placed across $R_a$ to measure the voltage drop. Adapted from Lambda Scientific [5].

A fixed resistor $R_a$ and a voltmeter across it are used to determine the resistance $R_B$ by attaching the setup to the simplified Wheatstone bridge circuit. The digital voltmeter measures the voltage drop across $R_a$, and $R_B$ is derived using the relationship:

$$\frac{V_+ - V}{V} = \frac{R_B/2}{R_a} \tag{3}$$

Where $V$ is the voltmeter reading, the equation is then rearranged to give:

$$R_B = 2R_a \frac{V_+ - V}{V} \tag{4}$$

When the magnetic field is zero:

$$R_0 = 2R_a \frac{V_+ - V_0}{V_0} \tag{5}$$

With both $R_B$ and $R_0$ determined, these values can be used to calculate the magnetoresistance using Equation (2), allowing the experiment to proceed.

# 3 Methods

As discussed in the Introduction, this experiment investigates the magnetoresistance properties of two GMR sensors: the multilayer GMR sensor and the spin-valve sensor. This investigation is conducted by measuring the resistance $R_B$ as a function of the applied magnetic field $B$. We aim to determine key parameters such as the sensitivity, linear range, and maximum relative resistance change by analysing the sensor responses. Table 1 summarises the theoretical properties of the sensors, including the precise resistance $R_a$, which is used in the calculations.

Table 1: Types of available sensors and their specifications. Adapted from King's College London [4].

| | |
|---|---|
| **Multilayer GMR Sensor** | Linear range: $0.15 - 1.05\,\mathrm{mT}$<br>Sensitivity: $30.0 - 42.0\,\mathrm{mV/V/mT}$<br>$\mathrm{MR_{max}}$: $10.4\%$<br>Precise resistor $R_a$: $1200\,\Omega$ |
| **Spin-Valve GMR Sensor** | Linear range: $-0.81 - 0.87\,\mathrm{mT}$<br>Sensitivity: $13.0 - 16.0\,\mathrm{mV/V/mT}$<br>Precise resistor $R_a$: $360\,\Omega$ |

The experimental setup consists of two main components: the Helmholtz coil unit and the control unit. The Helmholtz coil generates a uniform magnetic field $B$, while the control unit measures the sensor's voltage output $V$ in response to this field. The sensors are placed at the centre of the Helmholtz coils for measurements, with the connections configured according to the manufacturer's guidelines.

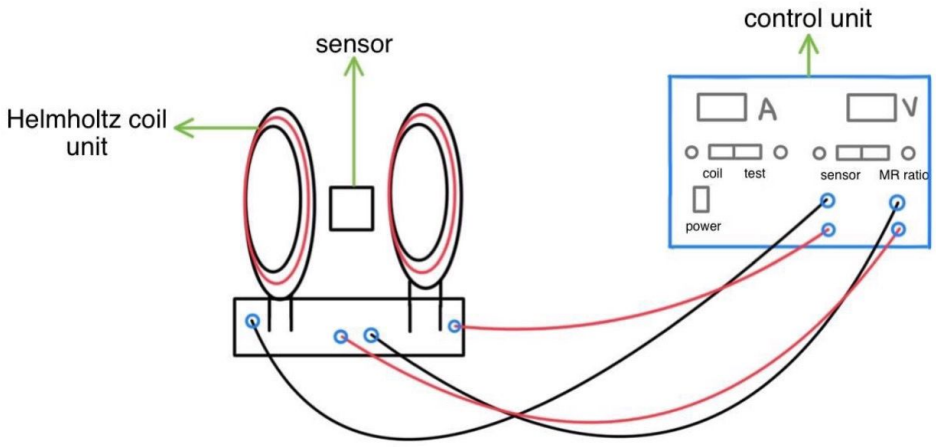


Figure 5: Schematic of the experimental setup for measuring magnetoresistance. On the left, two Helmholtz coils generate a magnetic field with a sensor positioned at the centre. The sensor can be either a multilayer GMR sensor or a spin-valve GMR sensor. On the right, the control unit displays the current supplied to the Helmholtz coils and the corresponding sensor output voltage. Wires connect the control unit to the sensor and the Helmholtz coil unit for precise measurements.

The control unit displayed the current supplied to the coils and the voltage output from the sensor. Using this voltage output and the precise resistance $R_a$ specific to the GMR sensor being used, as shown in Table 1, the resistances $R_B$ and $R_0$ were determined using Equations (4) and (5).

The magnetic field $B$ generated by the Helmholtz coil was calculated using the relationship [4]:

$$B = \frac{8\mu_0 NI}{5^{3/2} r}, \tag{6}$$

where:

- $\mu_0$ is the permeability of free space ($\mu_0 = 4\pi \times 10^{-7}\,\mathrm{T{\cdot}m/A}$),
- $N = 200$ is the number of turns in the Helmholtz coil,
- $I$ is the current supplied to the coils,
- $r = 0.1\,\mathrm{m}$ is the radius of each coil.

The magnetic field $B$ at each instance was calculated by substituting the known parameters and the current $I$ provided by the control unit. This data was then used to study the relationship between the resistance $R_B$ and the magnetic field $B$.

# 4 Procedure

## 4.1 Multilayer GMR Sensor

The multilayer GMR sensor was mounted at the centre of the Helmholtz coils. Initially, the coil current was set to zero using the control unit, and the corresponding output voltage $V_0$ was measured to determine $R_0$ (Equation (5)).

The current was then gradually increased in steps of 0.05 A, and the voltage $V$ was recorded at each step. At each current value, the current was held constant for a sufficient duration to allow the voltage to stabilize, thereby improving the precision of the measurements.

The process continued until the voltage readings became constant, indicating that the maximum magnetoresistance had been reached.

The uncertainty in the current was estimated to be 0.0005 A, calculated as half the smallest increment displayed on the digital meter. Similarly, the uncertainty in the voltage was determined to be 0.0005 V, following the same method.

## 4.2 Spin-Valve GMR Sensor

The Spin-Valve GMR sensor was mounted at the centre of the Helmholtz coils, replacing the multilayer sensor. Initially, the coil current was set to zero using the control unit, and the corresponding output voltage $V_0$ was recorded.

The coil current was then gradually increased in steps of 0.1 A, and the sensor output voltage $V$ was recorded at each step. At each current increment, the current was held

constant for a sufficient duration to allow the voltage readings to stabilize. The current was increased until it reached 1.2 A, at which point the current gradually decreased to zero in the same 0.1 A steps.

The cables supplying current to the Helmholtz coils were swapped to generate a magnetic field in the opposite direction. This ensured that the current flowed in the opposite direction, producing a magnetic field in the reverse direction. The current was then increased from 0.1 A to 1.2 A, similar to the previous process. However, due to the reversed polarity of the coils, these values were treated as negative current values.

At $-1.2$ A, the current decreased to zero in steps of 0.1 A. Finally, the cables were swapped back to their original configuration, and the current was increased again to 1.2 A and returned to zero, completing a full magnetic hysteresis loop.

The uncertainties in the current and voltage measurements were considered to be the same as in the previous part, with values of $\pm 0.0005$ A and $\pm 0.0005$ V, respectively, based on the resolution of the digital meters.

# 5 Results

## 5.1 Multilayer GMR Sensor

### 5.1.1 Magnetic Field $B$ vs. Relative Resistance Change $R_B/R_0$

The magnetic field $B$ was calculated using Equation (6), and the relative resistance change $R_B/R_0$ was determined using Equations (4) and (5). By substituting $V_+ = 5$ V (the supply voltage) and $V_0 = 1.6453$ V (the measured voltage when no current flows, corresponding to zero magnetic field), the formula for $R_B/R_0$ simplifies to:

$$\frac{R_B}{R_0} = \frac{(5 - V)}{V} \cdot 0.4904 \tag{7}$$

The resulting graph of $B$ vs. $R_B/R_0$ is shown in Figure 6.

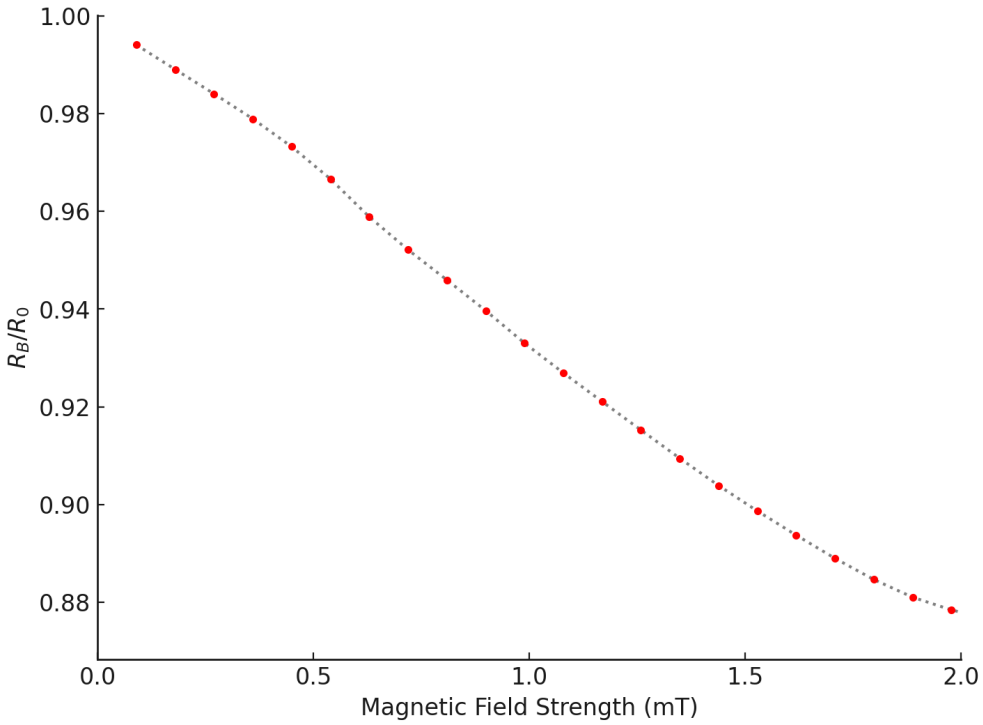


Figure 6: Relative resistance change $R_B/R_0$ as a function of magnetic field $B$ for the Multilayer GMR sensor. The error bars are too small to be visible.

The uncertainty in $B$ was calculated using error propagation as:

$$\Delta B = \frac{8\mu_0 N}{5^{3/2} r} \cdot \Delta I. \tag{8}$$

Here, $\Delta I = 0.0005\,\mathrm{A}$, as discussed previously in Section 4.

The uncertainty in $R_B/R_0$ was determined using the formula:

$$\Delta\left(\frac{R_B}{R_0}\right) = \left|\frac{\partial}{\partial V}\left(\frac{5-V}{V} \cdot 0.4904\right)\right| \cdot \Delta V \tag{9}$$

$$\Delta\left(\frac{R_B}{R_0}\right) = \frac{2.452}{V^2} \cdot \Delta V \tag{10}$$

where $\Delta V = 0.0005\,\mathrm{V}$, as discussed previously in Section 4.

The maximum magnetoresistance ($\mathrm{MR}_{\max}$) was determined using the formula:

$$\mathrm{MR}_{\max} = \left|\frac{R - R_0}{R_0}\right| = \left|\frac{R_B}{R_0} - 1\right| \tag{11}$$

The $R_B/R_0$ value, which turned out to give us $\mathrm{MR}_{\max}$, was $0.874 \pm 0.0004$.

Although higher $R_B/R_0$ values (e.g., 0.99) are observed in the graph, they do not represent the true maximum magnetoresistance. The magnetoresistance is determined using the absolute value of $R_B/R_0 - 1$. As a result, values farther from 1 on the $R_B/R_0$ axis yield larger absolute values when subtracted from 1.

Substituting into Equation (11), the maximum magnetoresistance was found to be $\mathrm{MR}_{\max} = 0.126 \pm 0.0004$.

The corresponding percentage value, including uncertainty, was calculated as $12.6 \pm 0.04\,\%$.

### 5.1.2 Voltage $V$ vs. Magnetic Field $B$

The relationship between the sensor output voltage $V$ and the magnetic field $B$ is shown in Figure 7. The linear region of the graph was identified from $B = 0.35\,\mathrm{mT}$ to $B = 1.4\,\mathrm{mT}$, as indicated by the black line.

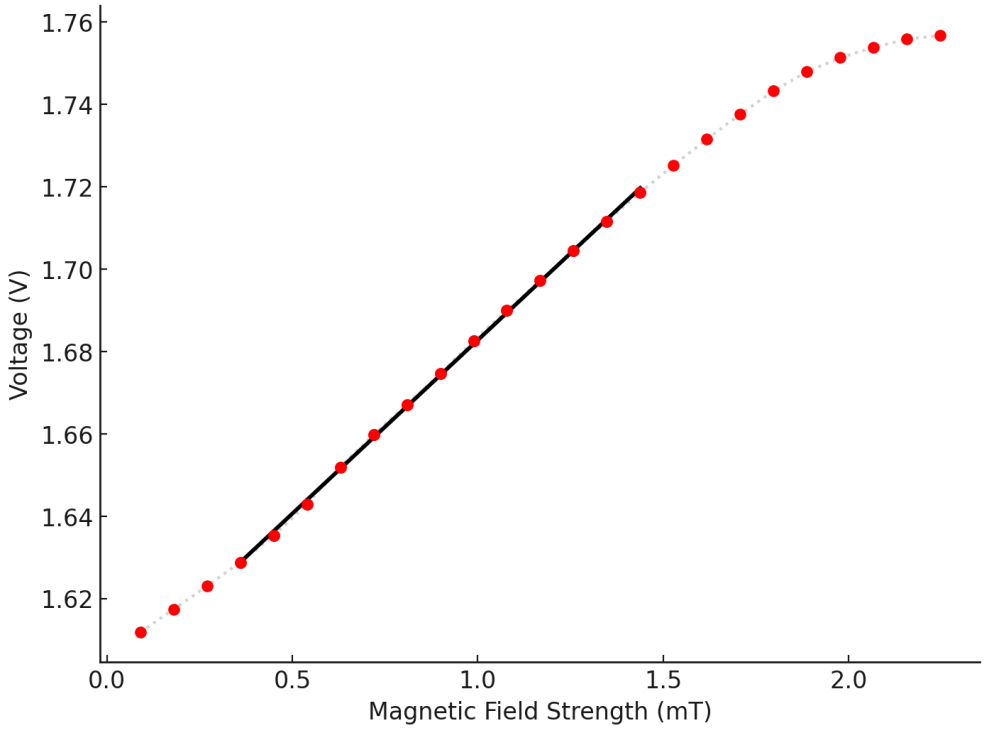


Figure 7: Voltage $V$ as a function of magnetic field $B$ for the Multilayer GMR sensor. The linear region (black line) extends from 0.35 mT to 1.4 mT. The error bars are too small to be visible.

The uncertainties in $B$ and $V$ are the same as those discussed in Equation (8) and Section 4, respectively.

The linear region of the graph was analyzed using the least squares method in Excel, yielding the following equation:

$$V = \alpha B + C, \tag{12}$$

where $\alpha = 83.60 \pm 0.72\,\mathrm{V/T}$ and $C = 1.63921 \pm 0.00074\,\mathrm{V}$.

The gradient $\alpha$ represents the voltage response to changes in the magnetic field $B$. The sensitivity $k$ was then calculated using the relationship:

$$k = \frac{\alpha}{V_+} \tag{13}$$

where $V_+ = 5\,\text{V}$. Substituting the value of $\alpha$, the sensitivity was found to be $k = 16.72 \pm 0.14\,\text{mV/V/mT}$.

The uncertainties in $\alpha$ and $C$ were determined using Excel's least squares fitting method.

### 5.1.3 Magnetic Hysteresis Loop: Voltage $V$ vs. Magnetic Field $B$

The magnetic hysteresis loop for the spin-valve GMR sensor was obtained by plotting the sensor output voltage $V$ against the magnetic field $B$, as shown in Figure 8. This graph demonstrates the characteristic hysteresis behaviour of the spin-valve sensor, revealing its response under forward and reverse magnetic field directions.

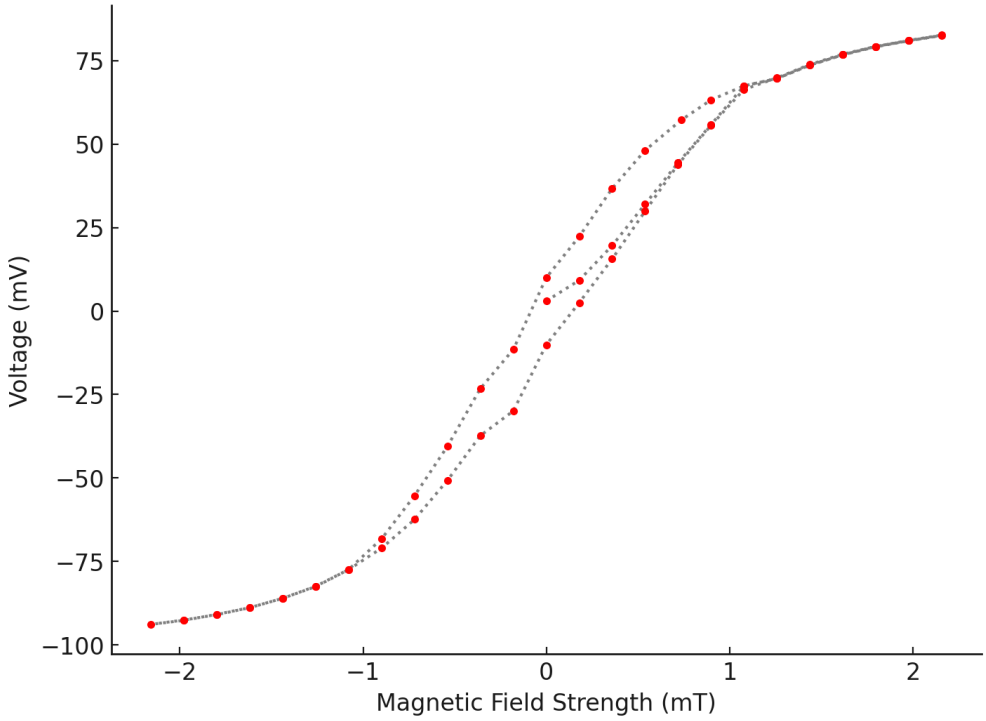


Figure 8: Magnetic hysteresis loop: Voltage $V$ as a function of magnetic field $B$ for the Spin-Valve GMR sensor. The error bars are too small to be visible.

The uncertainties in $V$ and $B$ were determined based on the resolution and calculation methods discussed earlier. The uncertainty in $V$ was found to be $0.0005\,\text{V}$, which corresponds to the resolution of the digital voltmeter, as described in Section 4. The uncertainty in $B$ was calculated using Equation (8), where the uncertainty in $I$ (used in the calculation of $B$) is $0.0005\,\text{A}$, as discussed in Section 4.

### 5.1.4 Linear Region Analysis: Sensitivity and Linear Range

From the $V$ vs. $B$ graph, a linear region was identified between $B = -0.8\,\text{mT}$ and $B = 0.8\,\text{mT}$. This region is isolated and displayed in Figure 9, where the fitted line represents the sensor's response within this range.

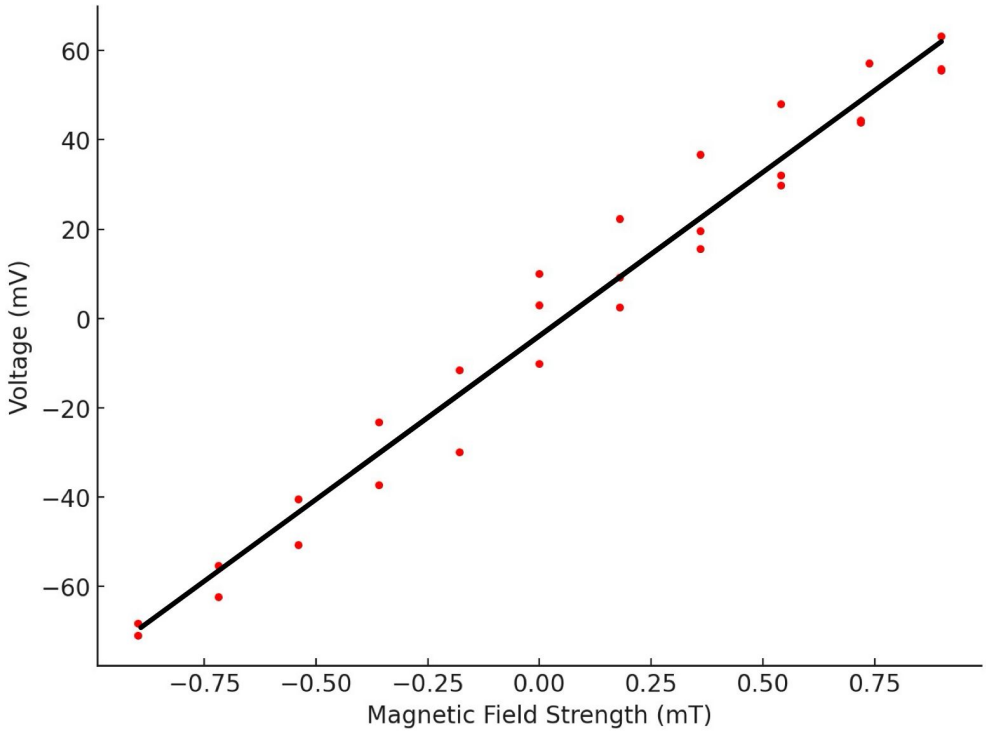


Figure 9: Linear region of voltage $V$ as a function of magnetic field $B$ for the Spin-Valve GMR sensor. The linear fit is shown in black. The error bars are too small to be visible.

The linear equation is given by:

$$V = \alpha B + C, \tag{14}$$

where $\alpha$ is the gradient, and $C$ is the y-intercept. Using the least squares method in Excel, the following values were obtained: $\alpha = 73.20 \pm 2.60\,\mathrm{V/T}$ and $C = -0.0039 \pm 0.4992\,\mathrm{V}$.

The sensitivity $k$ of the spin-valve GMR sensor was calculated from the gradient $\alpha$ using Equation (13), where $V_+ = 5\,\mathrm{V}$ is the supply voltage. Substituting the value of $\alpha$, we find $k = 14.64 \pm 0.52\,\mathrm{mV/V/mT}$.

# 6 Discussion

Table 2: Comparison of Theoretical and Measured Values for GMR Sensors

| Sensor Type | Property | Theoretical | Measured |
|---|---|---|---|
| **Multilayer GMR** | Linear Range (mT) | $0.15 - 1.05$ | $0.35 - 1.4$ |
| | Sensitivity (mV/V/mT) | $30.0 - 42.0$ | $16.72 \pm 0.14$ |
| | $\mathrm{MR}_{\max}$ (%) | 10.4 | $12.6 \pm 0.04$ |
| **Spin-Valve GMR** | Linear Range (mT) | $-0.81 - 0.87$ | $-0.8 - 0.8$ |
| | Sensitivity (mV/V/mT) | $13.0 - 16.0$ | $14.64 \pm 0.52$ |

The results for the multilayer GMR sensor revealed deviations from theoretical expectations, particularly in the behaviour observed at lower magnetic fields. In both the $B$ as a function of $R_B/R_0$ (Figure 6) and $B$ as a function of $V$ (Figure 7) graphs, the response exhibited non-linearity at the start. Theoretically, the linear region should begin at $B = 0.15\,\mathrm{mT}$, but in our measurements, linearity started much later at $B = 0.35\,\mathrm{mT}$. This delay indicates potential experimental issues, such as insufficient stabilization time for voltage readings at small magnetic fields or a systematic calibration offset in the setup.

Despite the non-linearity at the start, the measured linear range extended further to $B = 1.4\,\mathrm{mT}$, compared to the theoretical endpoint of $B = 1.05\,\mathrm{mT}$. While the overall range remained similar in magnitude (approximately $1.05\,\mathrm{mT}$), the observed shift towards higher fields suggests the presence of a zero-offset calibration error. This shift may have affected the determination of the maximum magnetoresistance ($\mathrm{MR}_{\max}$).

The measured $\mathrm{MR}_{\max}$ value was 12.6%, slightly higher than the theoretical 10.4%. Since $\mathrm{MR}_{\max}$ depends on saturation effects at higher magnetic fields, the initial non-linearity likely had minimal impact on this result. However, the systematic shift in the graph cannot be ignored as it could have influenced the point at which saturation was observed. In the end, we did observe that our $\mathrm{MR}_{\max}$ value was slightly deviated, which could have been a result of this offset.

The sensitivity of the multilayer GMR sensor was determined from the slope of the linear region in the $V$ as a function of $B$ graph (Figure 7) and was found to be $k = 16.72 \pm 0.14\,\mathrm{mV/V/mT}$. This value is significantly lower than the theoretical range of $30.0 - 42.0\,\mathrm{mV/V/mT}$. Theoretically, the line of best fit should have included the entire linear range starting from $B = 0.15\,\mathrm{mT}$. However, as discussed earlier, the graph did not exhibit linearity in this range, which may have been caused by a calibration offset or insufficient stabilization of voltage measurements at lower magnetic fields. Consequently, the line of best fit was affected, leading to a lower measured sensitivity value than the theoretical expectation.

The magnetic hysteresis loop observed in the $V$ as a function of $B$ graph (Figure 8) for the spin-valve GMR sensor exhibits three distinct voltage values at zero magnetic fields. While it may initially seem counterintuitive that multiple voltages can correspond to the same magnetic field, this behaviour arises from the hysteresis effect inherent to the spin-

valve structure. Hysteresis occurs because the magnetization of the sensor lags behind the applied magnetic field as it cycles through positive and negative values, leaving residual magnetization (remanence) even when the external field returns to zero.

Our experiment's initial measurement began at zero voltage and zero magnetic field. After reaching positive saturation and cycling back to zero field, a slight positive offset in the voltage was observed due to remanent magnetization. The voltage exhibited a slight negative offset when the magnetic field was reversed in the negative direction and returned to zero. Finally, after cycling back to positive saturation and reducing the field again, the voltage returned to its earlier positive offset. This behaviour underscores the nature of hysteresis, where the magnetization state depends on the current magnetic field and the sensor's magnetic history.

As illustrated in Figure 2, the spin-valve GMR sensor comprises a pinned ferromagnetic layer stabilized by an antiferromagnetic layer and a free ferromagnetic layer separated by a non-magnetic spacer. The pinned layer maintains a fixed magnetization direction, while the free layer dynamically aligns with changes in the applied magnetic field. This structural property causes the pronounced hysteresis effect observed in spin-valve sensors.

In contrast, multilayer GMR sensors can also exhibit hysteresis effects, but to a much smaller degree due to the absence of a pinned layer. Without a pinned layer, the magnetization of all layers responds more symmetrically to the applied field, making it harder to observe significant hysteresis behaviour.

The linear region of the $V$ as a function of $B$ graph (Figure 9) for the spin-valve GMR sensor was identified between $B = -0.8\,\mathrm{mT}$ and $B = 0.8\,\mathrm{mT}$. This range closely matches the theoretical values of $-0.81\,\mathrm{mT}$ to $0.87\,\mathrm{mT}$. Small deviations in identifying the boundaries could arise from slight inaccuracies during measurement or interpretation. Nevertheless, the agreement between experimental and theoretical values is strong.

The measured sensitivity $k$ was determined to be $14.64 \pm 0.52\,\mathrm{mV/V/mT}$. This value falls well within the expected theoretical range of $13.0 - 16.0\,\mathrm{mV/V/mT}$, indicating good agreement with the theoretical predictions for the spin-valve GMR sensor.

# 7 Conclusions

In this experiment, we investigated the magnetoresistance properties of two GMR sensors: the multilayer GMR and the spin-valve GMR. While the spin-valve GMR sensor results showed strong agreement with theoretical expectations, the multilayer GMR sensor exhibited notable deviations.

For the multilayer GMR sensor, the measured linear range was delayed, starting at $0.35\,\mathrm{mT}$ instead of the theoretical $0.15\,\mathrm{mT}$, and extended to $1.4\,\mathrm{mT}$. As discussed earlier, this shift likely resulted from a calibration offset or insufficient stabilization time for voltage measurements at smaller magnetic fields. Additionally, the non-linearity observed at the start of the graph affected the line of best fit, leading to a measured sensitivity of $16.72 \pm 0.14\,\mathrm{mV/V/mT}$, significantly lower than the expected $30.0 - 42.0\,\mathrm{mV/V/mT}$. Despite these limitations, the measured $\mathrm{MR_{max}}$ value of $12.6 \pm 0.04\,\%$ was reasonably close to the theoretical 10.4%, suggesting that the initial deviations less impacted saturation effects at higher magnetic fields.

The spin-valve GMR sensor, on the other hand, demonstrated results that closely matched theoretical predictions. The magnetic hysteresis loop observed in the $V$ vs. $B$ graph reflected the expected behaviour of the spin-valve structure, where remanent magnetization caused multiple voltage values to occur at zero magnetic fields. This behaviour arises from the lagging magnetization response of the sensor due to its pinned and free ferromagnetic layers, as illustrated in Figure 2. The linear region was measured between $-0.8\,\mathrm{mT}$ and $0.8\,\mathrm{mT}$, aligning well with the theoretical range. The sensitivity of $14.64 \pm 0.52\,\mathrm{mV/V/mT}$ also fell within the expected theoretical range of $13.0 - 16.0\,\mathrm{mV/V/mT}$.

The discrepancies observed in the multilayer GMR sensor results highlight the importance of ensuring precise experimental procedures, such as proper calibration of the apparatus, sufficient stabilization time for voltage readings, and minimization of external magnetic field interferences. Notably, the spin-valve measurements were conducted more cautiously, which may explain the more substantial agreement with theoretical values. Additionally, the sensitivity of GMR sensors to external magnetic fields, including those from nearby electronic devices, emphasizes the need for a controlled experimental environment.

In conclusion, the experiment demonstrated the key characteristics of magnetoresistance in GMR sensors, with the spin-valve GMR sensor yielding more reliable results. Future experiment repetitions should incorporate the precautions taken during the spin-valve measurements to improve the accuracy of results for the multilayer GMR sensor.

# References


[1] Chang, L., Wang, M., Liu, L., Luo, S., and Xiao, P. *A brief introduction to giant magnetoresistance*. arXiv, 1412.7691, 2014. Available at: https://arxiv.org/abs/1412.7691.

[2] Chikazumi, S. *Physics of Ferromagnetism*. Oxford University Press, 1997.

[3] Griffiths, D.J. *Introduction to Electrodynamics*. Pearson, 2017.

[4] King's College London. *5CCP2100: Experimental Physics Laboratory Manual – Experiment on Magnetoresistance*. King's College London, 2024.

[5] Lambda Scientific. *LEAI-75 Theory: Magnetic Field and Its Applications*. Available at: https://lambdasys.com/uploads/info/LEAI-75-Theory.pdf. Accessed on [2/12/2024].

[6] Wikipedia. *Magnetoresistance*. Available at: https://en.wikipedia.org/wiki/Magnetoresistance.

[7] Wikipedia. *Giant Magnetoresistance*. Available at: https://en.wikipedia.org/wiki/Giant_magnetoresistance.

[8] Wikipedia. *Wheatstone bridge*. Available at: https://en.wikipedia.org/wiki/Wheatstone_bridge.

[9] Taylor, J.R. *An Introduction to Error Analysis: The Study of Uncertainties in Physical Measurements*. University Science Books, 1997.

[10] Tsymbal, E.Y., and Pettifor, D.G. *GMR Structures*. Available at: https://tsymbal.unl.edu/reference/giant_magnetoresistance/gmr_structures.shtml. Accessed on [2/12/2024].